Imaging input and output of neocortical networks *in vivo*

Jason N. D. Kerr*, David Greenberg, and Fritjof Helmchen*†

Department of Cell Physiology, Max Planck Institute for Medical Research, Jahnstrasse 29, D-69120 Heidelberg, Germany

Communicated by Bert Sakmann, Max Planck Institute for Medical Research, Heidelberg, Germany, July 19, 2005 (received for review June 1, 2005)

Neural activity manifests itself as complex spatiotemporal activation patterns in cell populations. Even for local neural circuits, a comprehensive description of network activity has been impossible so far. Here we demonstrate that two-photon calcium imaging of bulk-labeled tissue permits dissection of local input and output activities in rat neocortex *in vivo*. Besides astroglial and neuronal calcium transients, we found spontaneous calcium signals in the neuropil that were tightly correlated to the electrocorticogram. This optical encephalogram (OEG) is shown to represent bulk calcium signals in axonal structures, thus providing a measure of local input activity. Simultaneously, output activity in local neuronal populations could be derived from action potential-evoked calcium transients with single-spike resolution. By using these OEG and spike activity measures, we characterized spontaneous activity during cortical Up states. We found that (*i*) spiking activity is sparse (<0.1 Hz); (*ii*) on average, only ≈10% of neurons are active during each Up state; (*iii*) this active subpopulation constantly changes with time; and (*iv*) spiking activity across the population is evenly distributed throughout the Up-state duration. Furthermore, the number of active neurons directly depended on the amplitude of the OEG, thus optically revealing an input–output function for the local network. We conclude that spontaneous activity in the neocortex is sparse and heterogeneously distributed in space and time across the neuronal population. The dissection of the various signal components in bulk-loaded tissue as demonstrated here will enable further studies of signal flow through cortical networks.

bulk loading | population imaging | presynaptic | sparse coding

Understanding how information is represented and processed in the mammalian neocortex requires measurement not only of single-cell dynamics but also of spatiotemporal activity patterns in identified networks of neurons *in vivo*. So far, optical imaging of intrinsic or voltage-sensitive dye signals has revealed spatiotemporal dynamics on the scale of cortical columns but has lacked cellular resolution (1). Extracellular recording methods have enabled simultaneous measurements from multiple cells but suffer from poorly defined cell identities, lack of spatial resolution, and are incapable of resolving nonactive neurons (2). These techniques thus fall short on providing a comprehensive description of cortical microcircuits. In particular, these methods cannot monitor the activation of afferent axons that represent the input into a particular local region. Of key importance to a further understanding of information processing in the neocortex will be a method that is capable of simultaneously resolving both input and output of cortical microcircuits with single-cell and single-spike resolution.

Here we apply recently developed techniques for two-photon calcium imaging of neocortical cell populations *in vivo* (3–5) to characterize neocortical activity during Up- and Down-state fluctuations, which are observed spontaneously during anesthesia (6, 7), sleep, and quiet wakefulness (8). We demonstrate that calcium imaging of neuronal somata reveals local spike patterns with single-cell and single-spike resolution. In addition, a prominent axonal-based calcium signal was found in the neuropil, providing a measure of local input. Analysis of the spatiotemporal distribution of spiking activity during spontaneous Up states revealed that spiking is sparse and heterogeneously distributed across neuronal populations. Furthermore, we show that the number of spikes depends on the level of driving input, as measured from the bulk neuropil calcium signal. Thus, calcium imaging of bulk-labeled tissue permits optical measurement of input–output relationships in local cortical circuits *in vivo*.

Methods

Surgical Procedures. All experimental procedures were carried out according to the animal welfare guidelines of the Max Planck Society. Wistar rats ($n = 35$; P25–36) were i.p. anesthetized with 2 g of urethane per kg of body weight. The animal skull was exposed and cleaned, and a metal plate was attached to the skull with dental acrylic cement. A 2- to 3-mm-wide craniotomy was opened above either the primary motor cortex or somatosensory cortex. The exposed cortex was superfused with warm normal rat ringer solution (135 mM NaCl/5.4 mM KCl/5 mM Hepes/1.8 mM $CaCl_2$, pH 7.2, with NaOH). The craniotomy was filled with agarose (type III-A, Sigma; 1% in normal rat ringer solution) and covered with an immobilized glass coverslip.

Labeling Procedures. Multicell bolus loading of neocortical cells with the calcium indicator Oregon green 488 1,2-bis(2-aminophenoxy)ethane-*N*,*N*,*N*′,*N*′-tetraacetate-1 (OGB-1) acetoxymethyl (OGB-1-AM; Molecular Probes) was performed as described in refs. 3–5. In most experiments, multicell bolus loading was performed in superficial layer 2/3 (L2/3). For specific loading of dendritic structures in layer 1 and L2/3, OGB-1-AM (1.4 mM) was slowly pressure-ejected into layer 5 of motor cortex for 10–15 min at 0.2–0.3 bar (1 bar = 100 kPa) with a micropipette tip 650–750 μm below the pia. This deep loading resulted in discrete labeling of layer 5 pyramidal neurons. Dendrites could be imaged 1–1.5 h after the injection. *In vivo* labeling of astrocytes was performed as described in ref. 4.

Two-Photon Microscopy. Two-photon imaging was performed by using a custom-built two-photon laser-scanning microscope as described in refs. 4 and 9. Excitation wavelength was ≈880 nm (Mira 900-F laser, Verdi-10 pump, Coherent, Santa Clara, CA). An Olympus (Melville, NY) 20× water-immersion objective lens (0.95 numerical aperture) was used.

Electrophysiology. Electrocorticogram (ECoG) was recorded with the tip of a 500-μm-diameter, Teflon-coated silver wire placed against the pial surface in one corner of the craniotomy. A reference electrode was placed over cerebellum through a small hole in the occipital bone. ECoG signals were acquired

Freely available online through the PNAS open access option.

Abbreviations: AMPA, α-amino-3-hydroxy-5-methyl-4-isoxazolepropionic acid; AP, action potential; ECoG, electrocorticogram; GYKI53655, 1-(4-aminophenyl)-3-methylcarbamyl-4-methyl-3,4,-dihydro-7,8-methylenedioxy-5H-2,3-benzodiazepine; IEI, interevent interval; OEG, optical encephalogram; OGB-1, Oregon green 488 1,2-bis(2-aminophenoxy)ethane-*N*,*N*,*N*′,*N*′-tetraacetate-1; OGB-1-AM, OGB-1-acetoxymethyl; L2/3, layer 2/3.

*Present address: Department of Neurophysiology, Brain Research Institute, University of Zurich, Winterthurerstrasse 190, CH-8057 Zürich, Switzerland.

†To whom correspondence should be addressed. E-mail: helmchen@hifo.unizh.ch.

with a custom-built AC-coupled amplifier (input impedance 1 MΩ; bandwidth 0.1 Hz to 8 kHz).

Patch-clamp recordings were performed from OGB-1-AM loaded L2/3 neurons in either cell-attached or whole-cell configuration. Cells were visually targeted by using a two-photon microscope. Open pipette resistance was 4–6 MΩ. Intracellular signals were recorded with an Axoclamp 2-B amplifier (Axon Instruments, Foster City, CA) and digitized with a CED1401*plus* (Cambridge Electronic Design, Cambridge, U.K.).

Pharmacology. To locally block postsynaptic activity, we applied the specific α-amino-3-hydroxy-5-methyl-4-isoxazolepropionic acid (AMPA)-type glutamate receptor antagonist 1-(4-aminophenyl)-3-methylcarbamyl-4-methyl-3,4,-dihydro-7,8-methylenedioxy-5H-2,3-benzodiazepine (GYKI53655) at 1 mM in normal rat ringer solution. A micropipette containing GYKI53655 was inserted in cortical L2/3. After a control imaging period of 3 min, GYKI53655 was continually pressure-ejected (0.3–0.4 bar) for 3 min. The application was ceased by either applying slight negative pressure (−0.01 bar) or by withdrawing the pipette. Imaging continued for a further 3–4 min.

Data Analysis. Calcium transients were measured by using frames made up of 64 × 128 or 32 × 128 pixels, with a line scan duration of 1–1.5 ms (15- to 31-Hz frame rate). OGB-1 fluorescence was averaged in regions of interest, including cell bodies or large areas devoid of cell bodies (neuropil). Background fluorescence was measured in unstained blood vessels. Signals were expressed as relative fluorescence changes ($\Delta F/F$) after background subtraction. Action potential (AP)-evoked calcium transients were detected with a template-matching algorithm that took advantage of their characteristic shape with a sharp rise followed by an exponential decay (10). See the supporting information, which is published on the PNAS web site, for more details on methods. All data are presented as mean ± SEM.

Results

Spontaneous Calcium Signals in L2/3 of Neocortex. We investigated spontaneous activity in the neocortex by using the recently developed multicell bolus loading technique for calcium indicator loading of cell populations *in vivo* (3). The membrane-permeable calcium indicator OGB-1-AM was pressure-ejected through a glass pipette into L2/3 of either motor cortex or barrel cortex in anaesthetized rats. Typically 1 h after dye injection, all cells within a radius of several hundred microns were labeled (Fig. 1*A*). Notably, not only cell bodies were stained but also the neuropil, which consists of dendrites, axons, presynaptic boutons, and glial processes. This staining pattern indicates that various cellular compartments had taken up calcium indicator dye. Neuropil staining was diffuse with no discernible structures, presumably because of the lack of contrast between similarly loaded subcellular compartments.

Unspecific loading by using the multicell bolus loading technique necessitates a dissection of the various calcium signal components. We previously showed that astrocytes can be identified *in vivo* by using the red fluorescent dye sulforhodamine 101 (4). This marker enables counterstaining of the astrocytic network and discrimination between the distinct calcium dynamics in astrocytes and neurons, respectively (Fig. 1). As in our previous study we observed slow calcium oscillations on the minute time scale in identified astrocytes (mean half duration, 75 ± 23 s; n = 15 cells and 5 animals). In contrast, neurons displayed spontaneous but infrequent calcium transients of short (<1 s) duration with fast onsets and exponential decays, resembling AP-evoked calcium transients observed *in vitro* and *in vivo* (9, 10). Most notably, large fluorescence changes were also present in the surrounding neuropil (Fig. 1*B*). Plotting the time course of mean fluorescence intensity in large regions of interest not containing cell somata revealed intensity

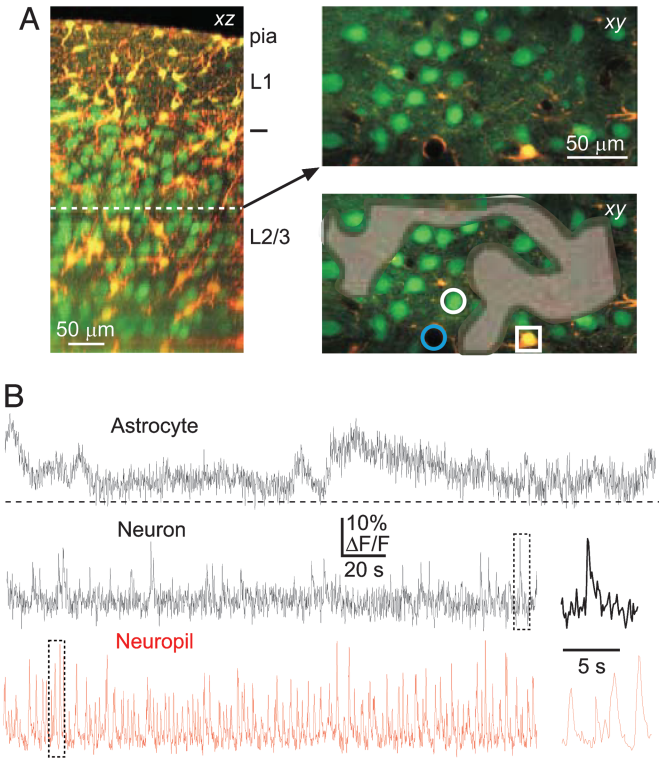

Fig. 1. Spontaneous calcium transients in cell somata and neuropil of bulk-loaded neocortical L2/3. (*A*) (*Left*) Side projection of OGB-1-loaded cells in the motor cortex. Astrocytes (yellow) were counterstained with sulforhodamine 101. (*A*) (*Right*) (*Upper*) Two-photon image 250 μm below pial surface showing neurons (green), astrocytes (yellow), and surrounding neuropil loaded with OGB-1. (*Lower*) Same area as *Upper* showing regions of interest: neuron (white circle), astrocyte (white square), neuropil (shaded gray), and blood vessel lumen for background (blue circle). (*B*) Simultaneous calcium transients from identified astrocyte (*Top*), neuron (*Middle*), and neuropil (*Bottom*) recorded over several minutes. (*Inset*) Note the sharp transients with fast onset and exponential decay (black) and ongoing neuropil signal on expanded time scale (from boxes).

fluctuations of 10–30% amplitude at frequencies in the 0.5–1 Hz range (0.56 ± 0.12 Hz, n = 5 animals). These fluctuations were above the intrinsic noise level of our imaging system, suggesting that they might represent a bulk measurement of calcium signals in neuropil structures. Before further characterizing spontaneous activity, we therefore addressed two crucial issues: (*i*) whether single APs can be detected in individual neurons and (*ii*) what the origin of the neuropil fluctuations is.

Single APs Are Resolved in Bulk-Loaded Tissue. To determine the sensitivity of our measurements of neuronal calcium transients we performed simultaneous cell-attached recordings (Fig. 2). Individual L2/3 neurons were targeted with a patch pipette filled with the red fluorescent dye Alexa Fluor 594, and a Gigaohm seal was formed (Fig. 2*A*). Subsequently, spontaneous APs were recorded extracellularly while somatic calcium transients in the same cell were simultaneously measured (Fig. 2*B*). At the end of the recording, a whole-cell configuration was established to verify which neuron had been recorded. To quantify the reliability of spike detection, we analyzed the fraction of optically detected individual APs and short bursts of a few APs (Fig. 2*C*). Overall, 97% of single APs and 100% of bursts were detected (95 single APs, 46 doublets, 6 triplets, and 4 quadruplets; n = 14 cells and 12 animals) (Fig. 2*E*). The calcium-transient amplitude correlated with the number of APs (R^2 = 0.81; see Fig. 4*D*) (11, 12). The average amplitude of single-AP evoked transients was 10.0 ± 0.9% and the mean decay

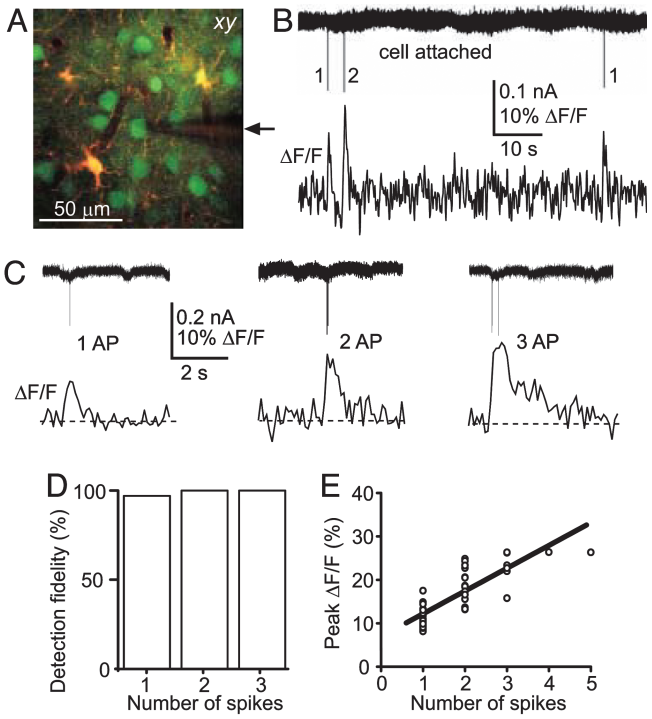

Fig. 2. Single AP-evoked calcium transients are detected in bulk-loaded tissue. (*A*) Overlay of OGB-1-loaded neurons (green) and astrocytes (yellow). The cell-attached recording was obtained from the center neuron (arrow indicates pipette containing 5 μM Alexa Fluor 594). (*B*) (*Upper*) Current trace from cell-attached recording showing spontaneous spikes from neuron depicted in *A* (number of spikes are indicated). (*Lower*) Simultaneously recorded somatic calcium transients corresponding to single APs as well as AP doublet. (*C*) Examples of somatic calcium transients (lower traces) evoked from spontaneous single APs, double APs, and triple APs from cell-attached recordings (upper traces). (*D*) Fidelity of spike detection confirmed with simultaneous cell-attached current recordings. The fraction of optically detected single APs and bursts of APs is shown. (*E*) Calcium transient amplitude as a function of the number of APs as detected from simultaneous cell-attached current recordings.

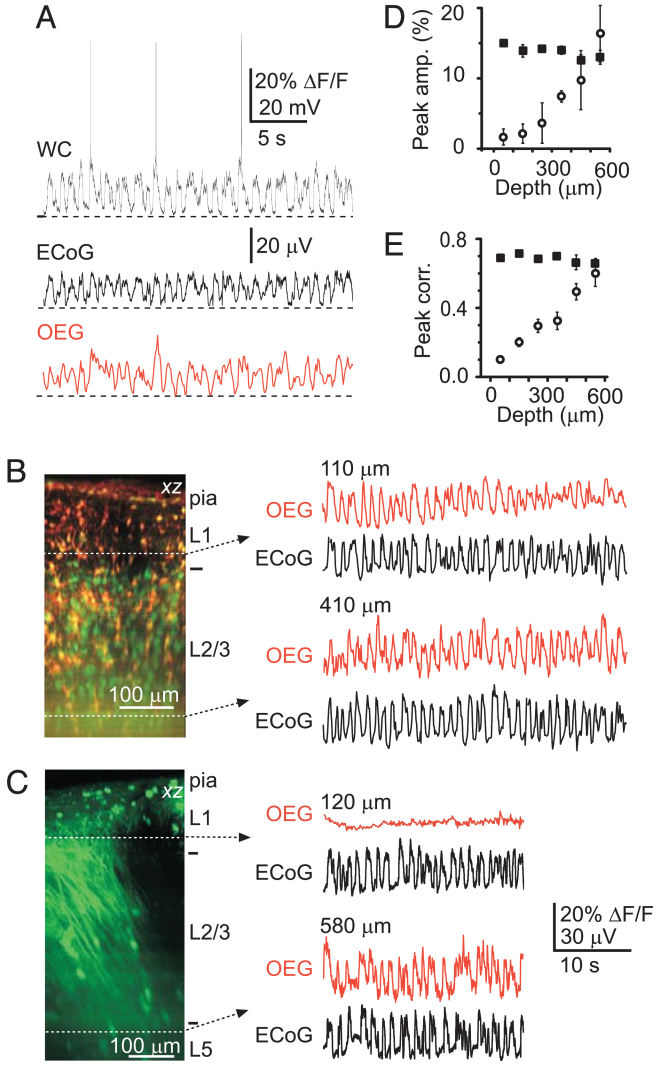

Fig. 3. Neuropil fluctuations are highly correlated with ongoing electrical activity. (*A*) Simultaneous measurement of membrane potential from a L2/3 pyramidal neuron using whole-cell (WC) recording, ECoG, and neuropil fluorescence fluctuation (OEG). (*B*) (*Left*) Side projection of cells superficially loaded with OGB-1 depicting depth from pia that neuropil signals were collected (dotted white lines). (*Right*) Ongoing OEG fluctuations (red) from different depths correlated with electrical ECoG signals (black). (*C*) Dendrites contribute little to OEG fluctuations. (*Left*) Side projection of OGB-1-loaded dendrites originating from layer 5 neurons using deep-loading technique (see *Methods*). (*Right*) Simultaneous ECoG recording (black) and OEG recording from dendrites (red). The lower traces show a recording near to the site of initial dye ejection (imaging depth indicated). (*D*) Peak amplitudes of neuropil calcium transients in superficially loaded cortex (■) and deeply loaded cortex (○). (*E*) Plot of peak correlation of neuropil and ECoG fluctuations at different depths when OGB-1 is loaded into L2/3 (■, $n = 5$ animals) or discretely loaded into layer 5 (○, $n = 5$ animals).

time constant was 0.82 ± 0.42 s ($n = 10$ transients and 5 animals). Bursts of two or more APs resulted in larger calcium transients (mean amplitude for doublets 15 ± 2%; decay time constant 1.01 ± 0.3 s; $n = 10$ transients and 5 animals). We conclude that AP activity is reliably resolved with single-cell and single-AP resolution by using calcium imaging of bulk-loaded tissue. This makes it possible to optically extract AP patterns, representing "output" activity, in local neuronal circuits, providing an optical analogue to multiunit recordings but with the advantage that AP activity can be assigned to identified neurons.

Optical Encephalogram (OEG) Recording from Neuropil. To explore the origin of neuropil fluorescence fluctuations we combined *in vivo* two-photon imaging with ECoG and whole-cell recordings. In whole-cell recordings from individual cells in bulk-loaded tissue the membrane potential fluctuated between Up and Down states as typically observed in neocortical neurons (Fig. 3*A*) (6–8). This ongoing spontaneous activity was also apparent in the ECoG, which correlated with the intracellular recording (peak correlation, 0.79 ± 0.1; $n = 5$ animals) (7, 13). Neuropil fluorescence fluctuations were highly synchronous to this electrical activity indicating that they reflect ongoing Up and Down states (Fig. 3 *A* and *B* and Fig. 7). Cross-correlations revealed a tight correlation with both the ECoG and intracellular recordings (mean peak correlation of 0.70 ± 0.1 and 0.75 ± 0.1, respectively; $n = 5$ animals). For calcium indicator loading in L2/3, both the peak $\Delta F/F$ amplitude of neuropil fluctuations and the peak correlation with the ECoG did not depend on depth from pial surface (Fig. 3 *B*, *D*, and *E*). These findings corroborate the idea that fluctuations in the neuropil are caused by spontaneous calcium signals in its components and directly linked to ongoing electrical activity. Given the strong correlation with the ECoG we have termed the neuropil signal OEG.

OEG Originates from Axonal Structures. Neuropil in neocortex consists of >50% axons and presynaptic boutons, 30% dendrites and dendritic spines, and 10% glial processes (14). All these

structures potentially could contribute to OEG fluctuations. Astrocytes are unlikely to contribute because they display calcium oscillations on a much slower time scale (Fig. 1) (4). Moreover, the tight correlation between electrical activity and OEG points to a neuronal origin. The question arises whether the OEG represents mainly axonal (presynaptic) or dendritic (postsynaptic) calcium signals.

To address this question, we used two complementary approaches. First, we developed a variant of the bulk-loading technique in which dye was discretely pressure-ejected in layer 5, predominantly labeling deep cells and their apical dendrites that project to upper cortical layers (Fig. 3*C*; see *Methods*). This loading method enabled us to investigate the dendritic component of the OEG in isolation. By using deep loading, the OEG was absent or markedly reduced in superficial layers (Fig. 3*C*). Peak $\Delta F/F$ amplitudes were 1.7 ± 1.1% at a depth of 150 μm and 3.7 ± 2.9% at 350 μm, which was significantly lower than with superficial loading ($P < 0.001$ for 150- to 450-μm depth; $P < 0.01$ for 550-μm depth; $n = 5$ animals; paired t test) (Fig. 3*D*). Only at depths greater than 500 μm and near the injection site were OEG amplitudes comparable with superficial loading (16.3 ± 4.0%; $P > 0.05$ for 600- to 680-μm depth). Similarly, by using deep loading, the correlation peak between simultaneously recorded OEG and ECoG was significantly reduced in the superficial layers down to 400 μm but not further below (peak correlation 0.1–0.2 at 50- to 150-μm depth, 0.2–0.4 at 200- to 400-μm depth, and 0.6–0.75 at ≈600-μm depth) (Fig. 3*E*). These results demonstrate that dendritic calcium transients contribute little if at all to the neuropil fluorescence signal, suggesting that the OEG is mainly axonal in origin.

To further test this axonal origin hypothesis, we locally blocked postsynaptic activity with GYKI53655, a specific antagonist of AMPA-type glutamate receptors (15), which should minimally affect axonal calcium signals. Pressure ejection of 1 mM GYKI53655 through a micropipette into L2/3 did not change the amplitude of ongoing OEG fluctuations in this area ($P = 0.87$; $n = 4$ animals) (Fig. 4 *A* and *B*). As a control, the postsynaptic blocking effect of the antagonist was obvious in the simultaneously measured pattern of spontaneous AP-evoked calcium transients (Fig. 4*A*). During antagonist application, the mean frequency of calcium transients significantly decreased (0.038 ± 0.005 Hz before and 0.014 ± 0.003 Hz with GYKI53655; $P < 0.001$, paired test; $n = 4$ animals) (Fig. 4*C*) but recovered to preantagonist levels after termination of drug application (0.046 ± 0.002 Hz; $P > 0.05$).

Taken together, these findings show that OEG fluctuations predominantly originate from axonal structures, presumably reflecting the bulk average of AP-evoked calcium transients in presynaptic boutons and axons activated during the Up-state periods. Thus, the OEG can be considered a measure for volume-averaged "input" activity to the particular local region.

APs Are Uniformly Spread Throughout Cortical Up States. *In vivo* calcium imaging in bulk-loaded tissue thus permits measurement of input and output neuronal activity in local cortical areas. We used this approach to characterize ongoing spontaneous activity in the neocortex on a population level. We first investigated the temporal structure of AP activity during Up states. In whole-cell recordings from L2/3 pyramidal neurons, APs occurred with a uniformly distributed temporal delay with respect to the onset of Up states (Fig. 5*A*). To investigate whether such a uniform distribution holds true at the population level, we performed a similar analysis on the somatic calcium transients detected simultaneously in small neuronal populations (up to 40 neurons). Fig. 5*B* shows 20 consecutively recorded Up states, as resolved from the ECoG and aligned to their onset, and corresponding AP-evoked calcium transient patterns of 38 identified neurons. Note that not every Up state produced AP-evoked calcium transients within the recorded neuronal population. As in the whole-cell recordings, AP activity was spread over the entire Up state and was not confined to one particular period (Fig. 5*B*). Pooling the delays from onset of AP-evoked calcium transients for 220 Up states from five animals and temporally binning these results revealed no significant difference between the different time bins during the average Up-state time course ($P > 0.05$) (Fig. 5*C*). Cumulative temporal distributions of both electrically measured and optically detected AP activity were linear ($R^2 > 0.99$), indicating a uniform distribution.

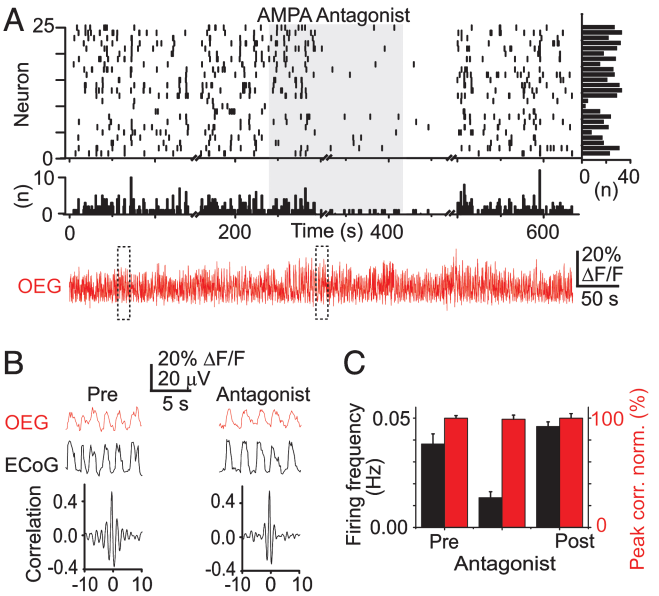

Fig. 4. Blocking postsynaptic spiking activity does not change OEG. (*A*) Spike-evoked calcium transients (raster plot) from 25 L2/3 neurons before, during (gray box), and after local pressure application of a specific AMPA receptor antagonist (1 mM GYKI53655). Shown are group activity during the same time periods (lower histogram; 1-s bins) and total activity of individual neurons (upper right histogram). Neuropil calcium fluctuations (red) recorded during the same period as raster plot. (*B*) Representative ECoG (black trace) and neuropil calcium fluctuation (red trace) periods and resulting cross correlations before and during antagonist application (taken from dotted boxes). (*C*) Summary of neuronal firing rates (black) and peak correlations (red) comparing preantagonist periods (pre) to antagonist periods and postantagonist periods.

Heterogeneity and Sparseness of Population Activity. We next aimed to determine the spatiotemporal distribution of the active subpopulation of neurons that participate in Up-states. We performed measurements in 90-s imaging periods from areas containing 20–30 neurons (Fig. 6*A*). To reveal the spatial pattern of activity we color-coded neurons according to the fraction of total Up-states during which they evoked a calcium transient. We found that the spatial organization of active neurons was not stable but displayed considerable heterogeneity over the time course of minutes (Fig. 6*B*). This heterogeneity indicates that spontaneous activity does not emerge exclusively in a particular subset of neurons but rather is generated by a continually changing subpopulation of neurons. Neurons also displayed heterogeneity with respect to their temporal activation. To test this we analyzed the distribution and coefficient of variance of interevent intervals (IEI) from individual neurons within a network (Fig. 6*E*). An event was defined as a calcium transient generated by one or more APs. The IEI distribution from individual neurons over 6 min (data not shown) as well as IEI distributions pooled from neuronal populations could be fitted by an exponential curve ($\tau = 15.7$ s, $R^2 = 0.98$) (Fig. 6*E*). IEI from individual neurons displayed high coefficient of variance values that ranged from 0.58 to 1.5 with a mean of 0.95 ± 0.04

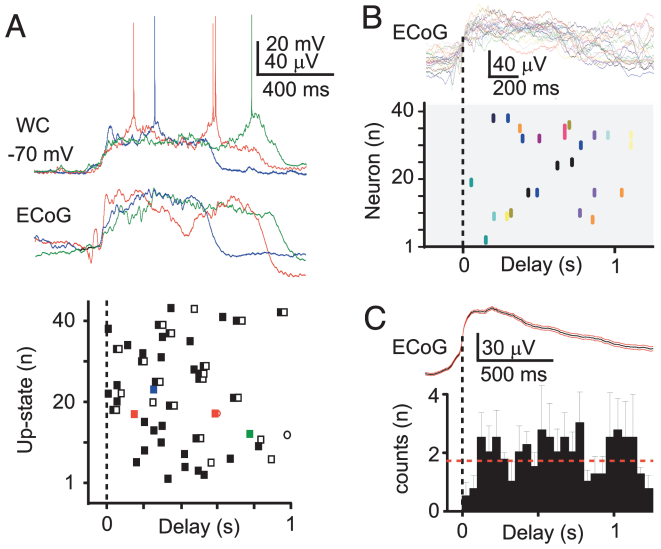

Fig. 5. Distribution of activity during Up states. (*A*) Overlay of ten spontaneous whole-cell Up states (*Upper*) and the simultaneous ECoG recordings (*Lower*) depicting variable timing of AP firing with respect to Up-state onset. Shown is the distribution of AP firing times from 43 Up states ($n = 5$ animals) with reference to Up-state onset (*Lower*). Indicated are the first (■), second (□), and third (○) APs. APs from upper membrane potential traces are indicated by colored symbols. (*B*) Raster plot of somatic calcium transients in 38 neurons imaged during 20 consecutive spontaneous ECoG Up states (overlay). Each line represents peak time of the activity, and the color is associated with the color of the different Up state (overlay). (*C*) Histogram of activity from 220 Up states from five animals showing average (red line) time of postsynaptic activity in relation to the average Up state time course (0.1-s bins).

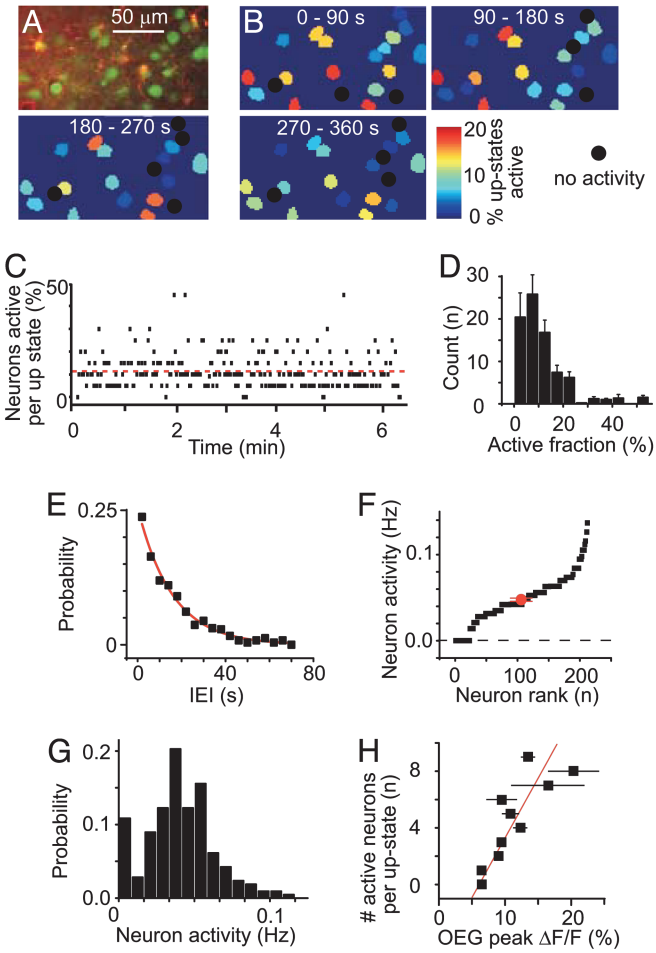

Fig. 6. Heterogeneous population spiking activity. (*A*) Fluorescence image showing the spatial distribution of the astrocytes (yellow) and OGB-1-filled neurons (green). (*B*) Pseudocolored representation of imaged area in *A* depicting the fraction of Up states in which neurons were active during a 90-s period. Activity scale is shown; neurons that were not active within this period are colored black. (*C*) Raster plot depicting the percentage of neurons from one area that produce spike-evoked calcium transients during consecutive Up states. Each point represents one Up state. The average activity is depicted by the red line. (*D*) Population histogram for the average percentage of neurons active during many Up states from five animals. (*E*) Population IEI distribution pooled from many imaging periods (exponential fit, red). (*F*) Range of firing frequencies in which 212 neurons were active over a period of 10 min; neurons were ranked according to their average activity (red point indicates mean). (*G*) Probability of spiking activity in a population of neurons from five animals (same data as in *E*). (*H*) Local input–output relationship. Relative $\Delta F/F$ changes in OEG fluorescence (presynaptic) during an Up-state transition calculated from the preceding Down state and plotted against the absolute number of postsynaptic spiking-related events (postsynaptic) during the corresponding Up state over the entire neuronal population.

($n = 5$ animals). These results suggest that AP activity during spontaneous ongoing activity in its simplest form is Poisson-distributed.

A major advantage of the imaging approach is that it permits the identification of nonactive cells, which enabled us to determine the fraction of cells that were active per individual Up state. In individual experiments, this fraction varied between 0% and 50% (Fig. 6*C*). Pooling many Up states from several animals yielded a skewed distribution with an average 10.6 ± 2.1% of neurons being active per Up state (183 neurons; 5 animals).

Neurons exhibited low rates of somatic calcium transients of between 0 and 0.14 Hz with a mean value of 0.048 ± 0.002 Hz ($n =$ 212 neurons and 11 animals) (Fig. 6*F*). These rates are consistent with the low rates of spontaneous APs observed in electrical recordings (cell-attached recordings: 0.05 ± 0.008 Hz, $n = 14$ neurons and 12 animals; whole-cell recordings: 0.05 ± 0.01 Hz, $n =$ 10 neurons and 9 animals; no significant difference between all groups, $P > 0.05$). Although some spontaneous calcium transients may have been evoked by bursts of several APs, these events were rare (<10%) and therefore had a negligible effect on the calculated rates using optical data. Of identified neurons, 11% did not show any calcium transients during the imaging period. One possibility is that these cells are interneurons, for which it is not clear whether single APs can be resolved. Ranking of all neurons according to their mean activity revealed a continuous, smooth distribution ranging from nonactive cells to cells with relatively high activity (Fig. 6*F*). Together, these results show that spontaneous AP activity in cortical L2/3 neurons is sparsely and heterogeneously distributed in space and time. The level of activity varies throughout the population but rather in the form of a continuum than in discrete groups of nonactive and active neurons.

Optical Recording of Local Input–Output Relationship. The OEG and the AP-evoked calcium transient patterns reflect input and output activity, respectively, in a local area of neocortex. A larger input, i.e., a stronger axonal activation, therefore should result in a larger output, i.e., generation of more APs. We tested this hypothesis by plotting the number of postsynaptic calcium transients in local groups of neurons against the amplitude of the OEG in the surrounding neuropil as a measure of the strength of axonal activation to this particular region. This analysis revealed a dependence resembling that of an input–output relationship (16, 17) with a threshold below which no APs were generated and an approximately linear relationship above threshold ($n = 5$ animals) (Fig. 6*H*). The ability to resolve axonal and cellular calcium signals in bulk-loaded tissue thus promises to be a useful tool for studying signal transformation in local neocortical networks.

Discussion

Optical Measurement of Output Activity. APs cause calcium influx through voltage-dependent calcium channels and evoke changes in intracellular calcium concentration. Hence, calcium imaging from cell populations can be used to extract spiking (output) patterns in neuronal networks, as has previously been shown in brain slices (18). Here, we extended this approach to *in vivo* conditions and demonstrated that single spikes can be optically detected after bulk loading with OGB-1. Such "optical multiunit recording" with single-cell resolution permits the extraction of spiking patterns in groups of up to 40 neurons at an ≈10-Hz frame rate. The temporal precision of this approach currently is limited because of the frame acquisition rate and the relatively slow (1 s) decay of the calcium signal, which causes calcium transients to merge as APs occur in rapid succession (10, 18). Taking into account the amplitude of AP-evoked calcium transients may improve the temporal accuracy of spike pattern extraction, because the amplitude depends on the number of APs (19) (Fig. 2*E*), their relative timing (20), and their spacing relative to the Up-state onset (21). Alternatively, faster dyes, such as voltage-sensitive dyes, could increase temporal resolution (1), but these dyes currently lack cellular resolution *in vivo*. In the current study, only a small fraction of events consisted of more than one AP, suggesting that the limited temporal resolution did not adversely affect the conclusions drawn.

Optical Measurement of Input Activity. A major finding of our study is the prominent spontaneous calcium signal in the neuropil, which we have termed OEG. We demonstrated that the OEG is predominately axonal in nature, consistent with the large fraction of neuropil volume occupied by axons and presynaptic boutons (14, 22). In our view, the OEG represents a volume-averaged signal, reflecting the summation of AP-evoked calcium transients in many activated axons. The OEG is thus complementary to the ECoG, which is thought to reflect synaptic potentials. Given that compound synaptic potentials reflect the mean rates of presynaptic input, the high correlation between OEG and ECoG is not surprising.

Two lines of evidence supported a presynaptic axonal origin of the OEG. First, dendrites in the neuropil contributed minimally to the OEG, which is in agreement with single-cell imaging experiments that reported no detectable calcium transients in apical dendritic trunks during subthreshold Up states (23). Although localized synaptic calcium transients in dendritic spines could contribute, they largely depend on NMDA receptor activation and therefore may be relatively small near resting membrane potential. Second, the OEG was not affected by locally blocking AMPA receptors, whereas the frequency of neuronal spike-induced calcium transients were clearly reduced. Although L2/3 pyramidal neuronal axon collaterals are located in close proximity to the neuron of origin and therefore may contribute to the OEG, no significant changes in the OEG were detected when spiking of local neurons was markedly reduced. In addition, neuronal firing was infrequent, but the OEG was continuous, and if the OEG did, in fact, rely on activity from local neuron axon arbors, then one would expect a more discontinuous OEG signal and less correlation with simultaneously recorded ECoG signals. Thus, OEG recording from the neuropil allows monitoring of volume-averaged input into the local neuronal network and correlation with simultaneous neuronal output activity.

Characteristics of Spontaneous Cortical Activity. Both electrical and optical recordings consistently revealed that individual neurons as well as populations of neurons display sparse spontaneous activity. Single neurons displayed low AP rates of <0.1 Hz, in agreement with previous *in vivo* studies (24, 25). On a population level, only a fraction (10%) of neurons was active during any given Up state, with this subset of active neurons changing over time. This temporal and spatial sparseness suggests a further capacity of the neocortex for encoding additional signals, e.g., sensory-evoked inputs, during Up-state periods. IEI distributions from neuronal populations were well approximated by a Poisson process. This stochastic behavior suggests that spikes do not explicitly depend on previous spiking times during spontaneous activity, which is in contrast to other studies that have reported spatial and temporal spiking structure in acute cortical slices (26, 27). Although these studies recorded transients from many more cells than in the present study, neurons were not distinguished from astrocytes, which could be important considering that astrocytes are gap–junction coupled and display calcium transients (4).

In summary, we have demonstrated that input and output activity can be measured in a local cortical region by using bulk calcium indicator loading. Furthermore, we observed a direct relationship between input and output because the amount of postsynaptic spiking activity depended on the strength of presynaptic axonal activity, measured by the OEG. The investigation of input–output relationships is of key importance for understanding signal processing in neuronal circuits (16, 28). Our optical approach, for example, could be used to investigate modulation of the gain of this transformation under various conditions of excitatory and inhibitory synaptic input (16). Furthermore, it should enable the study of input–output transformations during sensory input and how they are affected by varying levels of background activity such as they occur during different behavioral states.

We thank B. Sakmann and W. Denk for generous support; Marlies Kaiser for expert technical support; John D. Rolston for programming initial analysis software; and Drs. Tansu Celikel, Andreas Frick, and Rainer Friedrich for comments on an earlier version of the manuscript. We also thank Patrick Theer and Werner Göbel for useful discussions and help with microscope modifications.

1. Grinvald, A. & Hildesheim, R. (2004) *Nat. Rev. Neurosci.* **5,** 874–885.
2. Buzsaki, G. (2004) *Nat. Neurosci.* **7,** 446–451.
3. Stosiek, C., Garaschuk, O., Holthoff, K. & Konnerth, A. (2003) *Proc. Natl. Acad. Sci. USA* **100,** 7319–7324.
4. Nimmerjahn, A., Kirchhoff, F., Kerr, J. N. & Helmchen, F. (2004) *Nat. Methods* **1,** 31–37.
5. Ohki, K., Chung, S., Ch'ng, Y. H., Kara, P. & Reid, R. C. (2005) *Nature* **433,** 597–603.
6. Cowan, R. L. & Wilson, C. J. (1994) *J. Neurophysiol.* **71,** 17–32.
7. Lampl, I., Reichova, I. & Ferster, D. (1999) *Neuron* **22,** 361–374.
8. Petersen, C. C., Hahn, T. T., Mehta, M., Grinvald, A. & Sakmann, B. (2003) *Proc. Natl. Acad. Sci. USA* **100,** 13638–13643.
9. Waters, J., Larkum, M., Sakmann, B. & Helmchen, F. (2003) *J. Neurosci.* **23,** 8558–8567.
10. Helmchen, F., Imoto, K. & Sakmann, B. (1996) *Biophys. J.* **70,** 1069–1081.
11. Helmchen, F., Borst, J. G. & Sakmann, B. (1997) *Biophys. J.* **72,** 1458–1471.
12. Svoboda, K., Denk, W., Kleinfeld, D. & Tank, D. W. (1997) *Nature* **385,** 161–165.
13. Mahon, S., Deniau, J. M. & Charpier, S. (2001) *Cereb. Cortex* **11,** 360–373.
14. Chklovskii, D. B., Schikorski, T. & Stevens, C. F. (2002) *Neuron* **34,** 341–347.
15. Paternain, A. V., Morales, M. & Lerma, J. (1995) *Neuron* **14,** 185–189.
16. Chance, F. S., Abbott, L. F. & Reyes, A. D. (2002) *Neuron* **35,** 773–782.
17. Fellous, J. M., Rudolph, M., Destexhe, A. & Sejnowski, T. J. (2003) *Neuroscience* **122,** 811–829.
18. Smetters, D., Majewska, A. & Yuste, R. (1999) *Methods* **18,** 215–221.
19. Kerr, J. N. & Plenz, D. (2002) *J. Neurosci.* **22,** 1499–1512.
20. Callaway, J. C. & Ross, W. N. (1995) *J. Neurophysiol.* **74,** 1395–1403.
21. Kerr, J. N. & Plenz, D. (2004) *J. Neurosci.* **24,** 877–885.
22. Braitenberg, V. & Schüz, A. (1998) *Cortex: Statistics and Geometry of Neuronal Connectivity* (Springer, Berlin).
23. Waters, J. & Helmchen, F. (2004) *J. Neurosci.* **24,** 11127–11136.
24. Brecht, M. & Sakmann, B. (2002) *J. Physiol.* **538,** 495–515.
25. Margrie, T. W., Brecht, M. & Sakmann, B. (2002) *Pflugers. Arch.* **444,** 491–498.
26. Cossart, R., Aronov, D. & Yuste, R. (2003) *Nature* **423,** 283–288.
27. Ikegaya, Y., Aaron, G., Cossart, R., Aronov, D., Lampl, I., Ferster, D. & Yuste, R. (2004) *Science* **304,** 559–564.
28. Shadlen, M. N. & Newsome, W. T. (1998) *J. Neurosci.* **18,** 3870–3896.